Available online at www.sciencedirect.com
ScienceDirect
Journal of Nuclear Materials 367–370 (2007) 869–875
journal of nuclear materials
www.elsevier.com/locate/jnucmat

Thermal creep mechanisms in V–4Cr–4Ti pressurized tube specimens

D.S. Gelles *, M.B. Toloczko, R.J. Kurtz

Pacific Northwest National Laboratory, MS P8-15, P.O. Box 999, Richland, WA 99352, USA

Abstract

Pressurized thermal creep tubes of V–4Cr–4Ti have been examined following testing in the range 650–800 °C for tests lasting $\sim 10^4$ h to provide comparison with tests on similar tubes following irradiation. It is found in all cases that creep results from dislocation motion. But the mechanism changes with increasing temperature and lower stress from one controlled by the climb and interaction of individual dislocations, to one controlled by sub-grain boundary structure that is created by relaxation of the interacting dislocations to lower energy planar arrays. This change in mechanism corresponds to a change from power law creep to Newtonian creep such that the stress exponent drops from ~4 to ~1. Although it is possible to explain the Newtonian response as Nabarro–Herring or Coble creep, it appears more likely that behavior is due to Harper–Dorn creep, in which case the change in response occurs at the Peierls stress.

1. Introduction

Vanadium alloys such as V–4Cr–4Ti are being considered as first wall materials for fusion reactor applications. As part of that effort, pressurized tubes of V–4Cr–4Ti are being irradiated in fission reactors to provide predictions of irradiation creep response [1]. In coordination, thermal creep response is being studied by exposing similar pressurized tubes in a high vacuum furnace at temperatures between 650 and 800 °C in order to better understand irradiation creep response [2]. Results of that effort can be summarized in Fig. 1, showing thermal creep response as a function of applied stress for both uniaxial and biaxial (or pressurized tube) tests. The creep rates plotted represent estimates for the minimum creep rate observed, and it can be noted that based on this description, a change in creep mechanism is indicated for normalized levels, σ/G, below $\sim 2 \times 10^{-3}$ where G is the shear modulus, such that above that stress, the slope is ~4.3, and below ~0.84. Such behavior had previously been assumed to be due to Coble creep [3] and more recently, it was concluded that this linear response does not exist [4]. It is important to resolve these differences, because if Newtonian creep is misinterpreted, creep predictions will contain large errors at low stresses.

The purpose of the present work is to provide microstructural information from these pressurized tubes to better understand controlling mechanisms, and those data points labeled with identification

* Corresponding author. Tel.: +1 509 376 3141; fax: +1 509 376 0418.
E-mail address: ds_gelles@pnl.gov (D.S. Gelles).

0022-3115/$ - see front matter © 2007 Published by Elsevier B.V.
doi:10.1016/j.jnucmat.2007.03.067

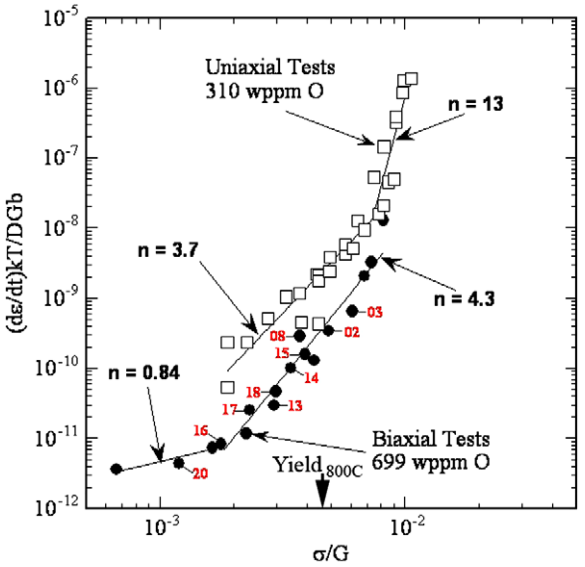

Fig. 1. Stress dependence of the normalized effective midwall creep strain rate for unirradiated vanadium alloys, with pressurized tube specimens chosen for microstructural examination identified by number.

codes in Fig. 1 correspond to tubes that have been destructively examined as part of that effort [5–7].

At low stresses, the steady state creep rate in single and polycrystalline materials can be directly proportional to stress, often described as Newtonian viscous flow. Three processes are now understood to control such behavior: Nabarro–Herring, Coble and Harper–Dorn creep. Furthermore, grain boundary sliding is understood to be required in order to accommodate Nabarro–Herring and Coble creep. Therefore, we report both on efforts to demonstrate grain boundary sliding based on optical metallography and to show examples of dislocation evolution as a function of applied stress.

2. Experimental procedure

Specimens selected for further examination are listed in Table 1. Detailed information on specimen preparation and creep testing procedures were reported previously [5,6]. One of the tubes failed during testing, and therefore, the applied stress was removed while at temperature. The vacuum furnace was shut down immediately upon detecting a tube failure so the time at temperature in the unstressed condition was minimal. The other two tubes did not fail and were allowed to cool while still under pressure. A section of as-received tubing was heated treated at 1000 °C for 1 h (designated AR) to provide comparison with deformed microstructures.

Optical metallography was based on a hydrofluoric–nitric acid etch:15 ml lactic acid, 15 ml HNO_3, and ~1 ml HF for ~1.5 min in order to better define grain boundary structure and (25 ml H_2O, 12.5 ml HNO_3, 12.5 ml HF for ~1 min [8]) to show precipitate stringers.

3. Results

3.1. Metallography

In an effort to differentiate between different creep mechanisms, grain aspect ratio change was investigated. Fig. 2 provides examples of the grain shapes in specimens AR, AR02, AR13, and AR20. All of the grain structures in these specimens appear equiaxed, with only a few examples of acicular grains elongated in the radial direction. It can be noted from Table 1, that effective midwall strains were 8.9%, 2.3%, and 12.7% respectively; however corresponding differences in grain elongation in the tube circumferential direction are not apparent from these images.

A longitudinal section of condition AR20 was examined following etching both to show grain structure and precipitate stringers [9] in order to determine if stringers could be used as markers to differentiate between operating creep mechanisms [10]. It should be noted that the longitudinal section is the only one that shows stringers but it is not ideal

Table 1
Test conditions for specimens examined

Specimen ID	Test temperature (°C)	Midwall effective stress (MPa)	Time to failure (h)	Effective midwall strain (%)	Comments on failure
AR	Not tested				
AR02	650	200	10601	8.9	Burst
AR13	700	119	9663[a]	2.3	Did not fail
AR20	800	48	6052[a]	12.7	Did not fail

[a] Specimen did not fail. The time listed is the total time at temperature.

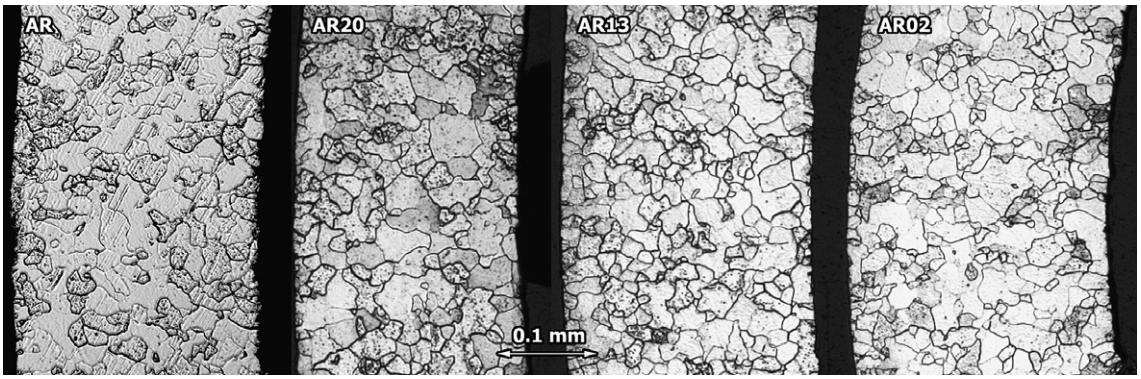

Fig. 2. Grain structure in V–4Cr–4Ti pressurized creep tubes.

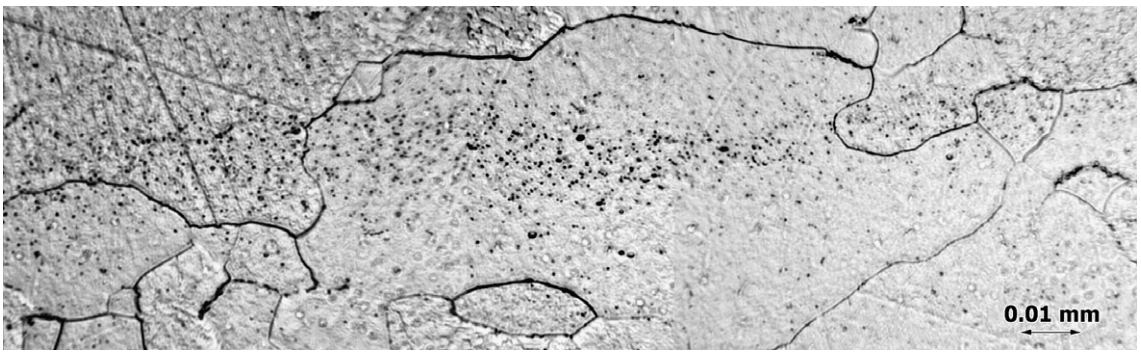

Fig. 3. Longitudinal stringer in specimen AR20.

for differentiating between creep mechanisms because creep tubes show negligible change in length. Few well defined stringers were found and only one extended over several grains. It is shown in Fig. 3. The stringer does not appear to show any off-set due to grain boundary mass transport, suggesting that Harper–Dorn creep is more likely than Nabarro–Herring or Coble creep.

In the course of examining for stringers in the longitudinal section of specimen AR20, several examples were found where precipitate particles appeared to collect on grain boundaries oriented in the longitudinal direction, whereas few boundaries oriented in the radial direction showed precipitate decoration. As hoop strain results in wall thinning, those boundaries oriented longitudinally would collect particles by diffusion processes involving grain boundaries. Four examples are provided in Fig. 4. Therefore, during creep at 800 °C in specimen AR20, a grain boundary mechanism involving either

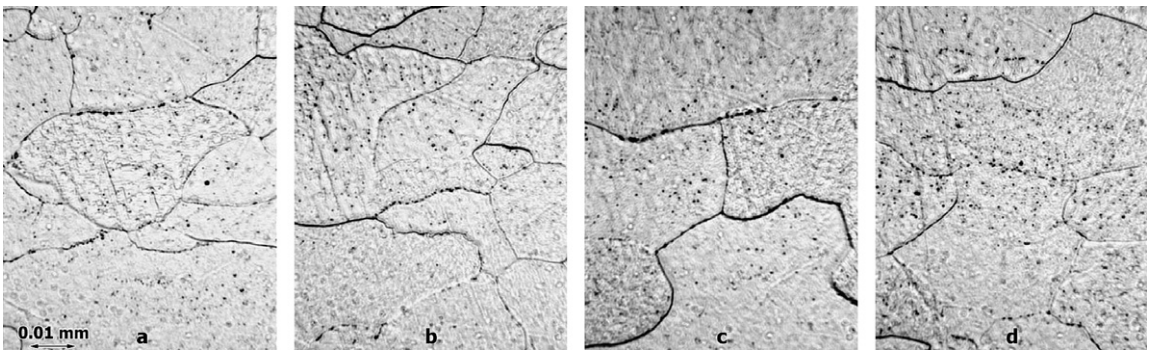

Fig. 4. Precipitation at grain boundaries in specimen AR20. The orientation is the same as in Fig. 3.

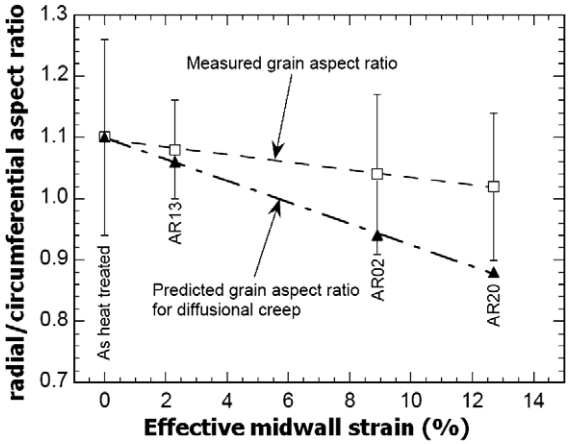

Fig. 5. Grain anisotropy in pressurized tubes as a function of midwall strain.

bulk diffusion or grain boundary diffusion, i.e., Nabarro–Herring or Coble creep, probably operated to collect particles at suitably oriented boundaries, but despite 12% strain, the impact was small.

3.2. Analysis of grain anisotropy

Grain aspect ratio measurements in tube radial and circumferential directions were made based on images similar to Fig. 2. Evidence for grain aspect ratio change was found as shown in Fig. 5. Note the bars bracketing the average values (open squares) for each specimen represent the range of measured aspect ratios and do not represent measurement error. It is noteworthy that the grain aspect ratio decreases approximately linearly with increasing midwall strain. In diffusion creep, the elongation of the grains will match the overall strain in the sample; whereas if deformation occurs predominantly by grain boundary sliding, there will be no significant grain elongation [10], so the grain aspect ratio will not change. The expected radial-to-circumferential aspect ratio can be estimated assuming none of the deformation is due to grain boundary sliding [11], with values (closed triangles) included in Fig. 5. These results suggest that grain boundary sliding may also contribute some fraction of the overall deformation for each of these specimens.

4. Discussion

It should be noted that our previous work has demonstrated a change in dislocation evolution for these conditions of V–4Cr–4Ti [5–7]. Examples at low magnification of the dislocation structures found are shown in Fig. 6. They demonstrate that specimens with high stress sensitivity show extensive dislocation evolution into complex tangles whereas sample AR20 with linear stress sensitivity when tested at 800 °C and low stress showed subgrain dislocation evolution indicative of significant dislocation motion and rearrangement during creep. This again suggests that grain boundary sliding or Coble creep might not be the operating creep mechanism. The possibility that it is Harper–Dorn creep that controls this behavior will now be considered.

In a companion effort [12], the literature is reviewed for the Harper–Dorn creep mechanism, and it is shown that a transfer from power law creep to Newtonian flow (showing a linear dependence with stress) will occur for Harper–Dorn, Nabarro–Herring and Coble creep, with the latter two mechanisms obliterating Harper–Dorn as grain size becomes small. Grain boundary sliding is considered to be a manifestation of Coble or Nabarro–Herring creep allowing accommodation. The transition stress below which Harper–Dorn is active is found to correspond to the Peierls stress, and therefore, the Harper–Dorn creep mechanism is based only on dislocation climb; when significant glide occurs, creep rates are non-linear with stress.

Fig. 1 includes an estimate of 185 MPa for the yield stress at 800 °C for a strain rate of 10^{-5} s^{-1} [13], shown on the σ/G axis. This value corresponds to about three times the stress at which the creep mechanism changes. Therefore, if Harper–Dorn creep is responsible for the change in mechanism indicated in Fig. 1, the Peierls stress for V–4Cr–4Ti at 800 °C is about one third the value of the yield stress.

4.1. Competing mechanisms

Further demonstration of Harper–Dorn controlled deformation for V–4Cr–4Ti at 800 °C and low stress is needed. The purpose of the grain aspect ratio and stringer study given in Figs. 1–4 was to differentiate between diffusion, grain boundary sliding and Harper–Dorn creep mechanisms as proposed by Langdon [10,14], but markers were not ideally oriented and were difficult to find. Based on stringer position across grain boundaries, Harper–Dorn Creep was indicated, but collection of particles on suitably oriented grain boundaries contradicted that conclusion and indicated either Nab-

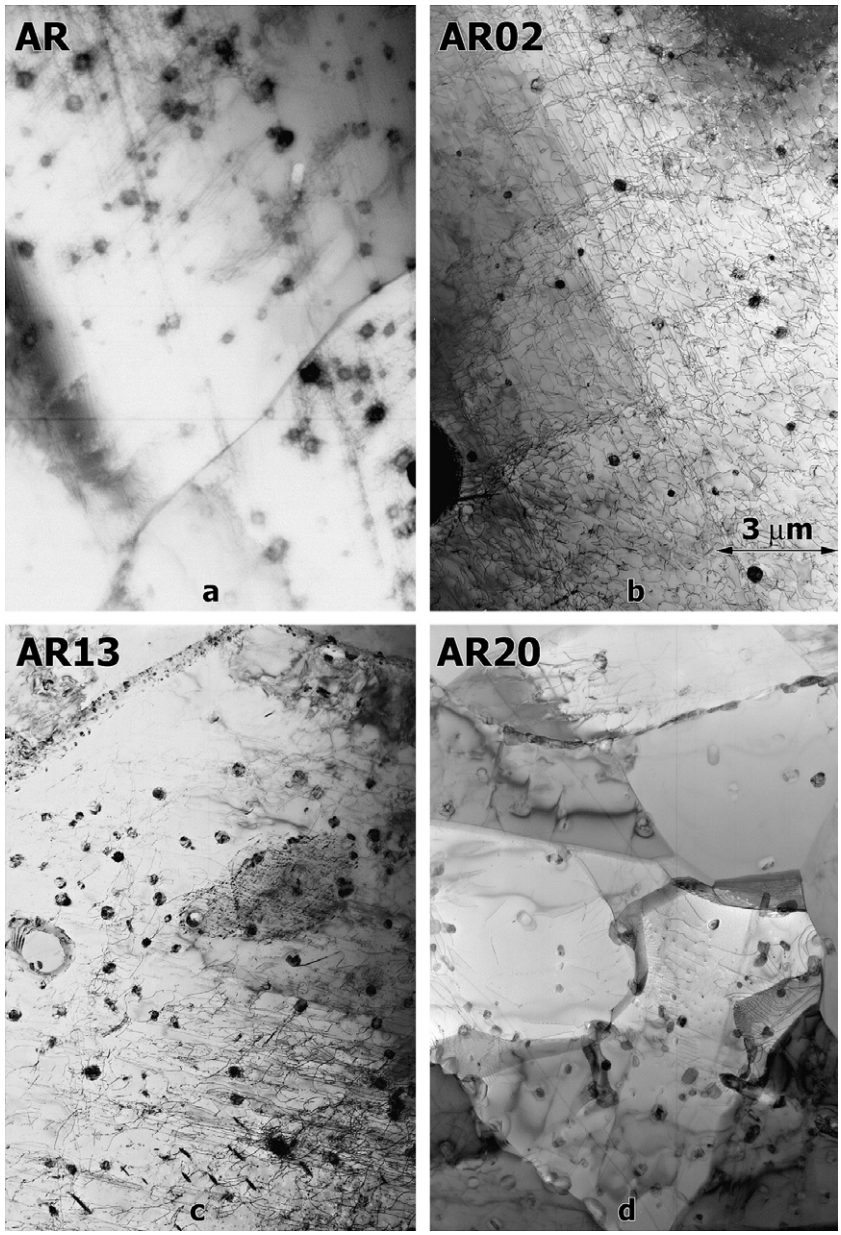

Fig. 6. Microstructures of pressurized tube specimens, (a) as heat treated, (b) AR02 tested at 650 °C/200 MPa, (c) AR13 tested at 700 °C/119 MPa and (d) AR20 tested at 800 °C/48 MPa.

arro–Herring or Coble creep was operating to some extent. Wang [15] has noted that Harper–Dorn creep should maintain a constant dislocation density irrespective of the operating stress, but the dislocation structures found in V–4Cr–4Ti pressurized tubes tested at 800 °C and low stress developed a recovered dislocation structure containing subgrains. However, Cadek [16] has concluded that subgrain development should be possible only if the grain size exceeds the subgrain size applicable for the applied stress. In the case of the present experiments, the grain size (~20 μm) is larger than the predicted subgrain size, $\lambda = 20b(G/\sigma) \approx 3$ μm. It can be argued that grain boundary sliding must allow accommodation that may take the form of dislocation evolution, which may account for the subgrain structure observed. Alternately, it may be argued that subgrains can behave as internal grain boundaries producing Nabarro–Herring or Coble creep.

Table 2
Parameters for theoretical creep predictions

Parameter	Harper–Dorn	Nabarro–Herring	Coble	Grain boundary sliding
A	$1.4(\tau_p/G)^2$	27	54	106
P	0	2	3	2
n	1	1	1	1

Consider instead prediction from theory. The steady state creep rate can be written for Harper–Dorn, Nabarro–Herring and Coble creep as follows:

$$\frac{\dot{\varepsilon}kT}{DGb} = A\left(\frac{b}{d}\right)^p\left(\frac{\sigma}{G}\right)^n, \quad (1)$$

where A is an appropriate dimensionless constant, D is the lattice diffusion coefficient, G is the shear modulus, b is the Burgers vector (0.262 nm for vanadium), k is Boltzmann's constant, d is the grain size ($\sim$20 μm), p is the appropriate grain size exponent, n is the stress exponent, and σ is the applied stress. The respective parameters are given in Table 2.

Experimentally, the linear stress dependence is found to begin at a normalized stress level $\sim 2\times10^{-3}$ for tests at 800 °C, yielding a normalized strain of $\sim 8\times10^{-12}$. For Harper–Dorn, the value of A depends upon the normalized Peierls stress, τ_p/G, which can be estimated from the procedure given by Wang [12] as 7.6×10^{-5} at 800 °C. Thus, the computed normalized creep strain at a stress of 2×10^{-3} for Harper–Dorn is 1.6×10^{-11}, for Nabarro–Herring it is 9.3×10^{-12}, for Coble creep it is 2×10^{-9}, and for grain boundary sliding creep it is 3.6×10^{-11}. The computed value for Nabarro–Herring creep is very close to the observed value in the biaxial creep tests, the computed creep rate for Coble creep is approximately 250 times larger than was observed, and the computed values for Harper–Dorn and grain boundary sliding creep are about 2–4 times higher than was observed. These calculations suggest that grain boundary sliding and Harper–Dorn creep mechanisms are more likely to describe pressurized tube creep behavior than Nabarro–Herring or Coble mechanisms, since the Nabarro–Herring mechanism is considered to be operable only at very high homologous temperatures and the Coble model significantly over predicts the observed steady-state creep rate. On the other hand, the pressurized tube creep data may be significantly influenced by interstitial impurities remaining in solution such that comparisons with models that do not include such effects may be difficult to interpret.

In summary, evidence can be found for all three Newtonian creep mechanisms and grain boundary sliding contributing to creep in V–4Cr–4Ti at 800 °C and low stress. Creep rate calculations predict Nabarro–Herring creep to be more favorable than Coble creep, but this seems unlikely at 800 °C. Metallographic evidence shows precipitate pile-ups on favorably oriented grain boundaries in agreement with both diffusional creep mechanisms. Microstructural evidence indicates that grain boundary sliding and Harper–Dorn creep should operate, supported by the grain aspect ratio measurements and the observed dislocation production and rearrangement. Most likely, each of these mechanisms plays a role in the deformation process, as a function of distance from active grain boundaries.

5. Conclusions

The mechanism controlling creep behavior at higher stresses/lower temperatures in V–4Cr–4Ti was shown to most likely be viscous glide controlled creep arising from the presence of Ti and Cr solid solution hardening. The predominant mechanism controlling creep behavior at lower stresses/higher temperatures should be grain boundary sliding or Coble creep, but given evidence for extensive dislocation production and rearrangement, Harper–Dorn creep may also contribute to the deformation process.

References

[1] R.J. Kurtz, K. Abe, V.M. Chernov, D.T. Hoelzer, H. Matsui, T. Muroga, G.R. Odette, J. Nucl. Mater. 329–333 (2004) 47.
[2] R.J. Kurtz, A.M. Ermi, H. Matsui, DOE/ER-0313/31 (2002) 7. Available from <http://www.ms.ornl.gov/programs/fusionmatls/pubs/semiannual.htm>.
[3] M. Li, S.J. Zinkle, J. ASTM Int. 2 (10) (2005), paper ID JAI12462.
[4] M. Li, T. Nagasaka, D.T. Hoelzer, M.L. Grossbeck, S.J. Zinkle, T. Muroga, K. Fukumoto, H. Matsui, M. Narui, J. Nucl. Mater., these Proceedings, doi:10.1016/j.jnucmat.2007.03.081.
[5] D.S. Gelles, DOE/ER-0313/31 (2001) 17. Available from <http://www.ms.ornl.gov/programs/fusionmatls/pubs/semiannual.htm>.
[6] D.S. Gelles, R.J. Kurtz, DOE/ER-0313/36 (2004) 2. Available from <http://www.ms.ornl.gov/programs/fusionmatls/pubs/semiannual.htm>.

[7] D.S. Gelles, M.B. Toloczko, L.E. Thomas, R.J. Kurtz, Further Observations on V–4Cr–4Ti Pressurized Creep Tubes, DOE/ER-0313/39, submitted for publication.
[8] D.T. Hoelzer, ORNL, private communication.
[9] D.T. Hoelzer, J. Bentley, 6th IEA and JUPITER Joint Workshop on Vanadium Alloys for Fusion Energy Applications, Tucson, AR June 21–22, 2002.
[10] T.G. Langdon, Met. Trans. 33A (2002) 249.
[11] D.S. Gelles, R.J. Kurtz, M.B. Toloczko, L.E. Thomas, DOE/ER-0313/39 (2006) 2. Available from <http://www.ms.ornl.gov/programs/fusionmatls/pubs/semiannual.htm>.
[12] D.S. Gelles, M. Toloczko, R.J. Kurtz, Comparison of Harper–Dorn and Irradiation Creep, DOE/ER-0313/41, submitted for publication.
[13] A.F. Rowcliffe, D.T. Hoelzer, S.J. Zinkle, DOE/ER-0313/26 (1999) 25. Available from <http://www.ms.ornl.gov/programs/fusionmatls/pubs/semiannual.htm>.
[14] T.G. Langdon, Mater. Sci. Eng. A 283 (2000) 266.
[15] J.N. Wang, Acta Mater. 44 (1996) 855.
[16] J. Cadek, Creep in Metallic Materials, Mater. Sci. Monographs, Elsevier, 1988, 151.